

pubs.acs.org/Macromolecules Article

# Surface Enrichment of Polymer-Grafted Nanoparticles in a Miscible Polymer Nanocomposite

Shawn M. Maguire, John Derek Demaree, Michael J. Boyle, Austin W. Keller, Connor R. Bilchak, Cherie R. Kagan, Christopher B. Murray, Kohji Ohno, and Russell J. Composto\*



Cite This: https://doi.org/10.1021/acs.macromol.2c00839



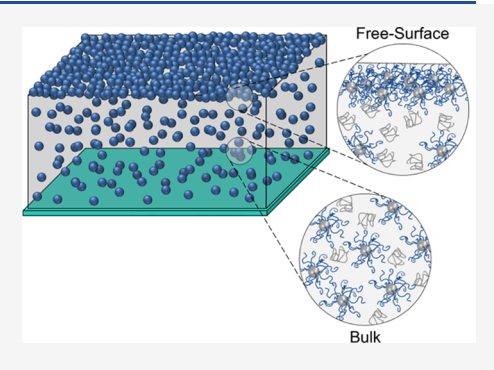
**ACCESS** I

III Metrics & More

Article Recommendations

SI Supporting Information

**ABSTRACT:** We show that the polymer-grafted nanoparticles (NPs) initially well-dispersed in a polymer matrix segregate to the free surface of a film upon thermal annealing in the one-phase region of the phase diagram because the grafted polymer has a lower surface energy than the matrix polymer. Using a combination of atomic force microscopy, transmission electron microscopy, and Rutherford backscattering spectrometry, the evolution of the poly(methyl methacrylate)-grafted silica NP (PMMA NP) surface excess in 25/75 wt % PMMA NP/poly(styrene-ranacrylonitrile) films is observed as a function of annealing time at 150 °C ( $T < T_{LCST}$ ). The temporal growth of the surface excess is interpreted as a competition between entropic contributions, surface energy differences of the constituents, and the Flory–Huggins interaction parameter,  $\chi$ . For the first time in a miscible polymer nanocomposite mixture, quantitative comparisons of NP surface segregation are



made with the predictions of theory derived for analogous polymer blends. These studies provide insight for designing polymer nanocomposite films with advantageous surface properties such as wettability and hardness and motivate the need for developing rigorous models that capture complex polymer nanocomposite phase behaviors.

#### INTRODUCTION

Historically, polymer nanocomposite (PNC) research has focused on controlling the bulk interactions between nanoparticles (NPs) and polymers to control the phase behavior. One successful approach to mediate this interaction is to graft polymer brushes to the surface of NPs. This brush can be tailored to interact either favorably or unfavorably with the polymer matrix depending on the complex interplay between entropic and enthalpic interactions. Although this interplay can lead to bulk PNC morphologies exhibiting well dispersed, stringed, and clusters of NPs, research focusing on controlling the surface properties of these PNCs is relatively nascent, in part, because surface composition is typically coupled to the bulk behavior. Early investigations of NP surface enrichment have already proven fruitful, where it has been shown that the addition of fullerene NPs to a miscible polymer blend can prevent film dewetting through interfacial NP enrichment.<sup>2</sup> Further advances in this area would benefit our ability to utilize PNCs in applications including self-healing interfaces and surfaces, hierarchical structured 3D nanocomposites for plasmonic applications,<sup>4</sup> and NP surface-enriched polymer composite scaffolds to promote bone repair. To control PNC surface properties, a new fundamental understanding is required beyond extending current models designed for polymer blends.

When grafted and matrix chains have similar composition (i.e., athermal case), grafted NPs have been shown to migrate

to the free-surface and substrate within a film, where the degree of segregation depends on NP size and relative molecular weights of the matrix (P) to graft (N) polymers (i.e., P/N). This preferential segregation of grafted NPs is entropic in origin and arises from the preference of chain ends over "mid-monomers" to locate on the surface. For  $P \gg N$ , longer matrix polymers experience a greater conformational entropy loss when confined near the surface compared to short, grafted polymers due to a smaller ratio of chain ends to mid-monomers. For an athermal system, neutron reflectivity experiments have shown that grafted NPs will segregate to the surface even when the ratio of P/N predicts "bulk" miscibility.<sup>7-10</sup> Further evidence of the importance of chain ends has been demonstrated in a nearly athermal blend of linear and branched polymers, where the branched polymer segregates on the surface. 6,11,12

Although both theory and experiments show that chain entropy favors grafted NPs to segregate to free surfaces and substrate interfaces in an athermal PNC film, the behavior of polymer-grafted NPs that are chemically distinct from the host

Received: April 22, 2022 Revised: July 27, 2022



matrix remains less understood. For A/B polymer blend films, where A and B are miscible, the free surface will generally be enriched with the lower-surface-energy component. 13 Here, the difference in surface energies between the A and B polymers allows the system to lower its total free energy by increasing the surface concentration of the lower-energy component. 14,15 In these miscible blends, the surface-energyinduced driving force can be enhanced or opposed by the bulk thermodynamics of the system, namely, the Flory-Huggins interaction parameter,  $\chi$ . For miscible systems,  $\chi$  is less than the critical value,  $\chi < \chi_c$ . Systems undergoing surface segregation can be categorized as having (1) moderate  $\chi$  and large surface energy difference ( $\Delta \gamma \gg 0$ ) as found in dSAN23/ SAN27 and dPS/PBrS, <sup>13,16,17</sup> (2) small  $\chi \approx 10^{-4}$  and small  $\Delta \gamma$  $\approx$  0.0001 J/m² characteristic of isotopic blends like dPS/PS and dPEP/PEP, <sup>15,18–22</sup> and (3) attractive interactions, where  $\chi$ < 0 and  $\Delta \gamma \gg 0$  like PS/PVME. <sup>20,23,24</sup> The balance between these two contributions is responsible for the amount of surface excess,  $Z^*$ , and the width of the surface layer. Case 3 is most relevant to this study. Namely, the segregation of the lower-surface-energy polymer (or brush-grafted NPs) is driven primarily by a difference in surface energy due to composition. This driving force for "demixing" competes with the bulk thermodynamic contributions (i.e., the Flory-Huggins interaction parameter) that favor uniform mixing of A and B. Although containing both enthalpic and entropic contributions, the surface energy difference between the brush and matrix polymer is dictated by their chemical difference; for our system, purely entropic contributions driving NP surface enrichment are relatively small.

In this article, we show that the surface of miscible 25/75 wt % poly(methyl methacrylate)-grafted silica NPs (PMMA NPs) and poly(styrene-ran-acrylonitrile) (SAN) PNCs is enriched with PMMA NPs and, for the first time in a miscible binary PNC mixture, attempt quantitative comparisons of this behavior with the predictions of current prevailing theories derived for polymer blends. The areal density of NPs is measured by atomic force microscopy (AFM) and found to saturate at a value of 517 NP/ $\mu$ m<sup>2</sup>, significantly greater than the as-cast value but less than that observed upon annealing in the two-phase region.<sup>25</sup> Cross-sectional transmission electron microscopy (TEM) images show a nearly monolayer of NPs on the free surface. Using grazing-incidence Rutherford backscattering spectrometry (GI-RBS), the surface excess of PMMA NPs is measured and found to saturate at 4.1 nm, which is ca. 50% less than the value observed for the same PNC annealed in the two-phase region.<sup>25</sup> Using the phase diagram, the Flory-Huggins interaction parameter, and the surface energy difference  $(\Delta \gamma)$  between PMMA and SAN (see Supporting Information), the surface enrichment for a PMMA/SAN blend is calculated and found to be much less than that measured experimentally for PMMA NP/SAN. This experimental study serves as motivation for the development of new theory that incorporates the appropriate bulk thermodynamic and surface energy contributions to the free energy for a PNC.

# **■ EXPERIMENTAL SECTION**

SAN ( $M_{\rm w}=118$  kg/mol,  $M_{\rm w}/M_{\rm n}=2.24$ , and  $T_{\rm g}=114$  °C, containing 33 wt % acrylonitrile) was provided by Monsanto and purified twice by adding a solution of SAN and chloroform [ $\geq$ 99.9%, for high-performance liquid chromatography (HPLC)] into methanol ( $\geq$ 99.9%, for HPLC) at a 1:10 volume ratio. After allowing SAN to

precipitate for 1 h, the solvent was removed, and the precipitant was dried for 48 h. Once dried, the SAN was redissolved in chloroform and precipitated with methanol once more. In order to achieve relatively high polymer brush molecular weights and grafting densities, silica NPs (15 nm diameter) grafted with PMMA brushes, denoted as PMMA NPs, were prepared using surface-initiated atom transfer radical polymerization due to the readily available synthesis methods.<sup>27</sup> The brush weight-average molecular weight and grafting density were 19 kg/mol and 0.7 chains/nm², respectively, as determined by thermogravimetric analysis (TGA, TA Instruments Q600 SDT) at a heating rate of 10 °C/min under argon flow between the temperatures of 25 and 550 °C. The glass transition temperature  $(T_{\sigma})$  of each polymer was measured using a differential scanning calorimeter (TA Instruments Q2000) between the temperatures of 25 and 150 °C. In all cases, two heating/cooling cycles were performed at a heating/cooling rate of 5  $^{\circ}$ C/min. The  $T_{\rm g}$  values were obtained from the second heating in order to eliminate any thermal history. The hydrodynamic radius of the PMMA NPs was determined to be 19 nm by dynamic light scattering (DLS, Malvern Zetasizer nano-s). Additionally, the ratio of matrix to the grafted chain molecular weights (P/N) is approximated to ca. 7.85. Details of TGA, differential scanning calorimetry (DSC), and DLS characterization of SAN and PMMA NPs are given in the Supporting Information of our previous work.<sup>26</sup> At all experimentally probed temperatures, the surface energy of PMMA is less than that of the SAN matrix (see Figure S1). EpoxiCure 2 epoxy hardener and epoxy resin were purchased from Buehler. N-type, oriented silicon wafers (dopant Ph, 10-20 Ω·cm resistivity,  $475-575 \mu m$  thickness, and single-side-polished) were purchased from Silicon Quest International. P-type, oriented silicon wafers (dopant B, 0.001-0.005  $\Omega$ ·cm resistivity, 500  $\mu$ m thickness, and single-side-polished) with a 300 nm wet thermal oxide layer were purchased from University Wafer.

25/75 wt % PMMA NP/SAN films were prepared by spin coating solutions (10 wt % solids in solvent) of the components in methyl isobutyl ketone (≥98.5%, certified ACS, Fisher Chemical) onto silicon; film thicknesses were *ca.* 450 nm. Samples were dried at 100 °C for 1 h to remove residual solvent. Following drying, the samples were annealed on a hot stage at 150 °C for various amounts of time under continuous argon flow and then quickly quenched below the glass transition temperature (*ca.* 120 °C) to "freeze" the concentration profile.

**Atomic Force Microscopy.** The PNC films were imaged in the tapping mode using an Agilent 5420 atomic force microscopy with non-contact tips (TAP300AL-G-50 radius of curvature < 10 nm, Ted Pella) as a function of thermal annealing temperature and time. All AFM images were processed using Gwyddion software. Radial autocorrelation functions of the 2  $\mu$ m  $\times$  2  $\mu$ m images were produced to discern the average center-to-center interparticle distances (IDs) of the grafted NPs at the film surface.

Transmission Electron Microscopy. To prepare the samples for TEM characterization, the 10 wt % PNC solutions were spin-coated (4000 rpm, 60 s) onto 1 cm × 1 cm silicon wafers with a 300 nm thermal oxide layer and then dried at 100 °C for 1 h to remove the residual solvent. Following drying and annealing at 150 °C for various amounts of time, the PNC films were lifted from their substrates. To do this, the edges of the substrates were scored with a diamond knife and then floated on a 1:5 vol % solution of NaOH (50% w/w NaOH) and deionized (DI) H2O. After lifting from its substrate, the films were transferred from the liquid-air interface of the NaOH solution to DI H<sub>2</sub>O and then onto Teflon. The specimens were then sandwiched between two pieces of tape, with an open window on one side to expose the free surface of the PNC. Next, the samples were embedded into two-part epoxy (see Supporting Information). Once the epoxy cured, ~70-100 nm-thick cross-sections of the PNCs were prepared by ultramicrotomy (Leica Ultracut S Ultramicrotome) with a room-temperature diamond knife. TEM characterization of the ultramicrotomed cross-sections, transferred onto carbon-coated TEM grids, was performed with a JEOL JEM-1400 TEM system operating at 120 kV.

Macromolecules Article pubs.acs.org/Macromolecules

Grazing-Incidence Rutherford Backscattering Spectrometry. To prepare samples for GI-RBS, the same 10 wt % PNC solutions used for AFM and TEM were spin-coated (4000 rpm, 60 s) onto 1 cm × 1 cm silicon wafers with no thermal oxide layer and then dried using the aforementioned procedure. After thermal annealing at 150 °C for various amounts of time, ca. 450 nm-thick samples were examined by GI-RBS using an incident beam of 2 MeV He+ ions produced by a National Electrostatics 5SDH-2 positive ion accelerator. The GI-RBS geometry consisted of an incident ion beam of 60° off the surface normal and an exit angle of 65°, resulting in a 175° backscatter. After obtaining the GI-RBS spectra, the counts versus channel profiles were translated into counts versus depth using in-house software and an energy calibration of 1.709 keV/channel with an offset of +95 keV, obtained from a 10 nm AuPd calibration sample. See Supporting Information for GI-RBS profile fitting details.

# ■ RESULTS AND DISCUSSION

100

To directly observe surface enrichment of PMMA NPs in a 25/75 wt % PMMA NP/SAN PNC, AFM was used to quantify the particle number density on the surface as a function of annealing temperature and time. Figure 1a,b shows represen-

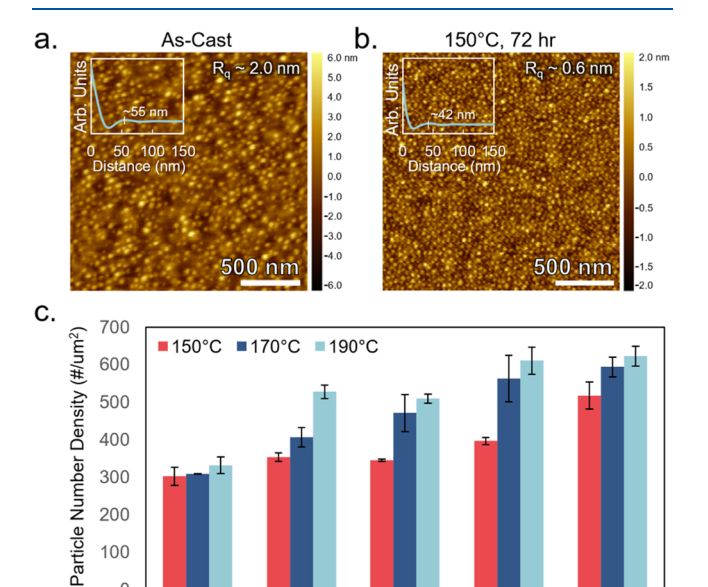


Figure 1. Surface morphology evolution of 25/75 wt % PMMA-NP/ SAN. AFM height images of the (a) as-cast and (b) annealed film at 150 °C after 72 h (4320 min). The insets are autocorrelation functions of the AFM images, revealing lower values of interparticle separation upon annealing. Additionally, the root-mean-square roughness indicates a smoother surface upon annealing. (c) Increase in the NP number density upon annealing at 150, 170, and 190  $^{\circ}\text{C}$  as a function of annealing time. Annealing at 150 °C is in the one-phase region of PMMA NP/SAN, whereas 170 and 190 °C correspond to the two-phase region. Parts of this image were adapted from ref 24 with permission from the American Chemical Society.

180

Annealing Time (min)

1440

4320

30

tative AFM images of the PNC surface with the height scale to the right of each image. The as-cast PNC (Figure 1a) shows uniformly dispersed PMMA NPs with an average center-tocenter ID of ca. 55 nm based on the peak in the images' autocorrelation function (Figure 1a inset). This value is in good agreement with small-angle X-ray scattering measurements (ca. 53 nm), suggesting a good dispersion of NPs.<sup>26</sup> A root mean square roughness  $(R_q)$  of ~2.0 nm is observed. Upon annealing in the one-phase region at 150 °C for 72 h, a

qualitative increase in the number density of NPs on the free surface is observed. This is supported by the images' autocorrelation function (Figure 1b inset), which displays a peak at ca. 42 nm. Correspondingly, a decrease in the rootmean-square roughness ( $\hat{R}_q \sim 0.6$  nm) is observed. This decrease in surface roughness has been discussed in recent work that investigated the wetting behavior of PMMA NPs in a binary PMMA-NP/SAN PNC. 25 Figure S2 shows AFM line profiles passing across the centers of the grafted NPs for samples before and after annealing at 150 °C. The center-tocenter distances obtained directly from line profiles are in good agreement with the values determined from the respective autocorrelation functions (Figure 1a,b).

Although the autocorrelation functions from AFM images suggest an increase in NP packing on the free surface, image analysis has been performed to quantify the number density of PMMA NPs as a function of annealing temperature and time (see Supporting Information). Figure 1c plots the NP number density versus annealing time up to 72 h at 150 °C. Additionally, Maguire et al. recently tracked the surface wetting behavior during simultaneous wetting and phase separation (i.e., two-phase region) in the same PNC, and their data are plotted here for reference at T = 170 and 190 °C. 25 For PNC films at 150 °C, Figure 1c shows that the surface enrichment of PMMA NPs increases with increasing annealing times. At the longest time (72 h), the NP number density is  $517 \pm 36$  NP/  $\mu$ m<sup>2</sup>, which is 1.7× greater than the value for the as-cast film,  $302 \pm 24 \text{ NP}/\mu\text{m}^2$ . Interestingly, for PNCs annealed in the two-phase region, the number density of NPs increases rapidly at short times and approaches plateau values of 593  $\pm$  26 and  $620 \pm 25 \text{ NP}/\mu\text{m}^2$  at 170 °C and 190 °C, respectively. Here, it is important to reiterate that in the one-phase region,  $\chi$  and  $\Delta \gamma$ compete with one another for NP surface enrichment. In contrast,  $\chi$  and  $\Delta \gamma$  mutually enhance surface wetting in the two-phase region. Therefore, a higher NP number density for films annealed in the two-phase region is expected. Importantly, however, this work, coupled with the previous work by Maguire et al., 25 is the first series of experiments to demonstrate and quantify such behaviors in grafted NP PNCs.

To simultaneously observe the internal morphology and surface layer, TEM cross-sectional images of the 25/75 wt % PMMA-NP/SAN film (ca. 450 nm) are presented before and after annealing at 150 °C as shown in Figure 2. Importantly, the as-cast samples exhibit a homogenous dispersion of the PMMA NPs within the SAN matrix (Figure 2a). However, for PNCs annealed at 150 °C, PMMA NPs diffuse to the free surface of the film to lower the system's overall free energy while remaining dispersed in the bulk. More specifically, the lower-surface-energy PMMA NPs are driven to the surface by both chain entropy and the surface energy difference between the PMMA graft and SAN matrix. These two driving forces compete with the bulk thermodynamics (i.e., the Flory-Huggins interaction parameter) that favors uniform mixing of PMMA-NP and SAN in the bulk. This surface excess of PMMA NPs is commensurate with the AFM results presented

As shown previously for polymer blends, the composition profile,  $\varphi(Z^*)$ , can be measured using depth profiling techniques such as secondary ion mass spectrometry. 18 In this work, we use GI-RBS to measure the composition profiles of the PMMA NPs as a function of depth within the film. Figure 3a shows a schematic illustration of the experimental configuration for GI-RBS. The sample is tilted 60° with respect

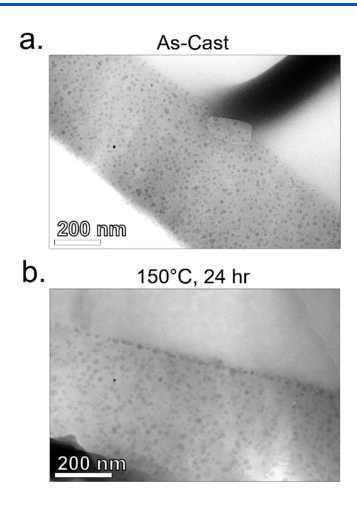


**Figure 2.** TEM cross-sectional images of 25/75 wt % PMMA-NP/SAN films as-cast (a) and annealed at 150 °C (b) for 24 h (1440 min). The internal morphology remains dispersed upon annealing with the emergence of a PMMA NP surface layer. Note: the black mark in (a) is a fold in the epoxy surrounding the PNC film.

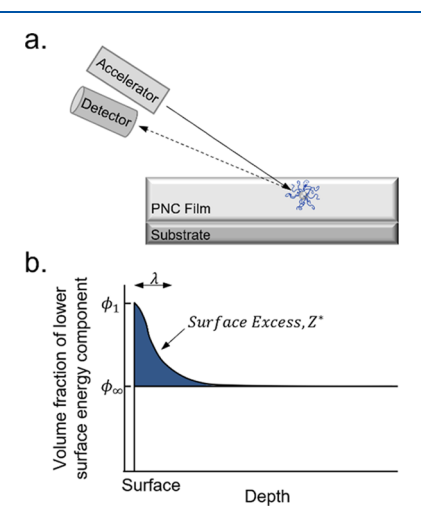


**Figure 3.** (a) Experimental configuration of GI-RBS for measuring NP surface excess. High-energy helium ions strike the PNC film at a grazing angle and are backscattered to a solid-state detector. The detector registers the energy of each backscattered helium ion, which directly correlates to the depth of each target element. (b) Schematic representation of the compositional profile of the surface enrichment of NPs at equilibrium along with key parameters.

to the incident beam to enhance spatial resolution in the near-surface region. Figure 3b schematically depicts the composition profile and visually defines the surface excess  $(Z^*)$ , the surface composition  $(\varphi_1)$ , the bulk composition  $(\varphi_\infty)$ , and characteristic thickness  $(\lambda)$ . For very thin films, one would expect the bulk composition  $(\varphi_\infty)$  to be less than that of the initial starting concentration due to conservation of mass. However, for thick films (such as those presented in this study), the surface excess is relatively small compared to the overall concentration of NPs in the system. Therefore, the overall decrease in bulk concentration (at equilibrium) is quite small and often beyond the sensitivity of the implemented methods, resulting in a  $\varphi_\infty$  comparable to that of the as-cast  $\varphi$ .

Using GI-RBS, the temporal evolution of the surface concentration profiles of PMMA NPs is measured in the one-phase region at 150 °C. Figure 4 shows concentration profiles (*i.e.*, counts) for the 25/75 wt % PMMA-NP/SAN

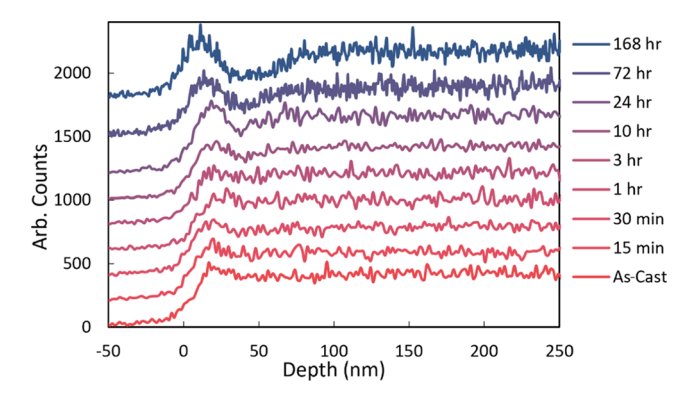


**Figure 4.** GI-RBS spectra of the silicon concentration depth profile in 25/75 wt % PMMA-NP/SAN films (ca. 450 nm) are shown at 150 °C as a function of annealing time. Spectra are shifted in counts for clarity. The surface peak near 0 nm represents an excess of PMMA NPs. Note: the depth profile is a convolution of instrument resolution and silica concentration profiles. The instrumental resolution broadens the counts near the surface, resulting in values below 0 nm.

films (ca. 450 nm) before and after annealing at 150 °C; these samples clearly show an enriched layer of PMMA NPs on the free surface. A very small peak is observed in the as-cast film, suggesting that some NPs locate on the free surface during drying and/or pre-annealing. This observation has been previously demonstrated as a kinetic effect that depends on the solvent evaporation rate and other factors. Except for the near-surface region, the PNC films display a uniform concentration of NPs as evidenced by the nearly constant counts above ca. 75 nm, consistent with the TEM image in Figure 2a. Beyond this point, we note that the growth of NPs to the free surface is purely due to difference in surface energies of the constituents and not due to solvent evaporation or film thickness changes during annealing. Importantly, the film thickness remains constant up to annealing times of 168 h at 150 °C. This was confirmed via GI-RBS depth profiles evident in Figure S5, where the increase in counts beginning around ca. 450 nm corresponds to the substrate interface. Immediately after annealing, the surface becomes enriched with a layer of PMMA NPs, represented by the appearance of a larger surface peak near 0 nm. For the 168 h case in Figure 4, the surface peak corresponds to a PMMA NP volume fraction of ca. 0.30 as calculated based on our GI-RBS profiles. It is worth noting that the corresponding bulk volume fraction is ca. 0.20. As discussed by Maguire et al., 25 the NP surface layer is immediately followed by a depletion zone formed when NPs adjacent to the surface diffuse to the surface. This depletion zone is most clearly observed for profiles after 24, 72, and 168 h of annealing. To our knowledge, this is one of the first studies, particularly for PNCs, which directly observes the formation of a depletion layer adjacent to the surface. Importantly, the formation of this depletion zone is a consequence of kinetics resulting from the diffusion process, where particles are taken from the near-bulk region and supplied to the interface, leaving behind regions void of NPs. Consequently, the depletion zone forms a concentration gradient toward the surface that drives NPs toward it. At "infinite" annealing times ( $t \gg 168$  h), NPs should have sufficient time to diffuse, resulting in the disappearance of the depletion zone and equilibration at the bulk concentration (excluding other factors such as NP jamming).

Using the GI-RBS spectra, we determine the integrated surface excess ( $Z^*$ ) of PMMA NPs at 150 °C as a function of annealing time. Using a previously published fitting procedure,  $Z^*$  can be extracted at each time, yielding the surface excess values shown in Figure 5. Here, we see that  $Z^*$  increases

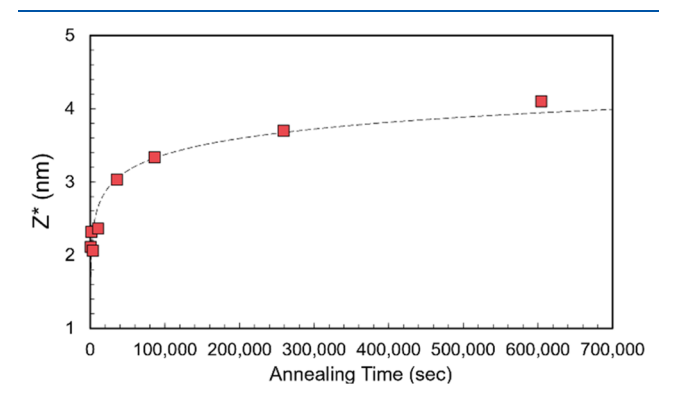


Figure 5. Surface excess of PMMA NPs plotted as a function of the annealing time. The dashed line is the best logarithmic fit to the data.

rapidly at short times and approaches a constant value at the longest annealing time (ca. 168 h). Due to the size of the grafted NPs (ca.  $R_{NP} = 19$  nm) and relatively low annealing temperature (~30 °C above the glass transition temperature of the PNC) the mutual diffusion of the PMMA NPs through the composite is expected to be slow. Additionally, attractive interactions between PMMA NPs and SAN can result in a bound layer of SAN on PMMA NPs, which can increase the effective NP size and further reduce NP diffusion. 32-36 Therefore, care has been taken to ensure that this PNC film has approached near equilibrium by annealing until only a small increase in the measured  $Z^*$  is observed, as demonstrated by the dashed line in Figure 5. Although bulk equilibrium may not be achieved due to slow rearrangement of NPs across the film, it is reasonable to assume that the surface excess is near the final value. We note that while performing experiments at a deeper quench (e.g., 130 °C) in the one-phase region of the phase diagram should result in a stronger driving force for surface enrichment, the time scales for NP diffusion to the PNC interfaces are expected to be orders of magnitude slower than those at 150 °C. As such, the annealing temperature was judiciously chosen to balance NP enrichment driving forces and kinetics. At the longest time (ca. 168 h), the PNC reached a near-equilibrium value of  $Z^* \cong 4.1$  nm. For the same PNC annealed in the two-phase region, the surface excess values were  $Z^* \cong 7.6$  nm and  $Z^* \cong 9.1$  nm after 24 h at 170 and 190 °C, respectively.<sup>25</sup> Since no models exist for predicting surface excess values for PNCs, we next apply a polymer blend model for comparison with our results.

Using the Schmidt–Bender model applicable to a polymer blend, Jones and Kramer showed that the surface excess of the lower-surface-energy component can be predicted using Flory–Huggins polymer theory and  $\Delta \gamma$  alone. Using their analytical expressions, the integrated surface excess and near-surface depth profiles of an analogous PMMA/SAN blend can be predicted with the following equation

$$Z^* = \frac{a}{3} \frac{1}{\sqrt{\chi_b - \chi}} (\sin^{-1} \sqrt{1 - \varphi_{\text{Bulk}}} - \sin^{-1} \sqrt{1 - \varphi_{\text{I}}})$$
(1)

where a is the statistical segment length,  $\chi_b$  is the value of the Flory–Huggins interaction parameter  $\chi$  on the coexistence curve, and  $\varphi_1$  and  $\varphi_{\text{Bulk}}$  are the compositions shown in Figure 3b. Here,  $\chi_b$  and  $\varphi_1$ , respectively, are given using the following equations

$$\chi_b = \frac{1}{N(1 - 2\varphi_\infty)} \ln \left( \frac{1 - \varphi_\infty}{\varphi_\infty} \right)$$
 (2)

$$\varphi_{l} = \frac{\varphi_{\infty} + t}{1 + t} \tag{3}$$

where *t* captures the surface and bulk driving forces for surface segregation and is given using the following equation

$$t = 9\left(\frac{\mu_1}{a}\right)^2 \frac{1}{\chi_b - \chi} \tag{4}$$

Here,  $\mu_1$  represents a surface chemical potential favoring the lower-surface-energy component (component 1) on the surface and is expressed as follows

$$\mu_1 = \frac{b^3}{kT} \Delta \gamma \tag{5}$$

where b is the size of the Flory–Huggins lattice cell. Using eqs 1-5,  $\Delta \gamma \sim 0.001 \text{ J/m}^2$ , and  $\chi \sim -0.039$ , 38 the surface excess of PMMA in a 25/75 wt % PMMA/SAN polymer blend is calculated. Here, the surface energy of a PMMA homopolymer is used to calculate  $\Delta \gamma \sim 0.001 \text{ J/m}^2$  based on PMMA homopolymer films and PMMA NP films of comparable molecular weights to those utilized in this study having similar water contact angles as measured through goniometry.<sup>39</sup> For PMMA, two molecular weights are considered: (1) PMMA with the same molecular weight as that of the PMMA NP brush (i.e., 19 kg/mol) and (2) PMMA with a molecular weight (ca. 491 kg/mol) having its radius of gyration commensurate with the radius of PMMA NPs (i.e.,  $R_g \cong$  $R_{\text{PMMA-NP}}$ ). For cases (1) and (2), the surface excess values of PMMA are  $Z^* \cong 0.70$  nm and  $Z^* \cong 0.79$  nm, respectively. These predictions are ca.  $5\times$  lower than the experimental  $Z^*$ value measured for the PMMA NP/SAN system.

We propose three plausible explanations for the underestimation of  $Z^*$ . (1) The model uses the Flory-Huggins equation for the free energy of mixing. The Flory-Huggins free energy of mixing for a grafted NP/polymer blend is known to differ from that of a pure polymer blend, as recently derived by Riggleman et al.40 (2) Jones and Kramer assume equal degrees of polymerization between constituents. Here, the degree of polymerization of the SAN matrix is ca. 6× larger than that of the PMMA graft. Importantly, this changes the bulk thermodynamics of the system, namely, increasing the free energy cost of mixing. <sup>23,41</sup> (3) The  $\Delta \gamma$  used in eq 5 may be slightly underestimated due to the use of the surface energy value of the PMMA homopolymer. The importance of chain ends has been previously discussed and may lead to lower surface energies of grafted NPs compared to those of their linear analogues. 6,11,12 Together, these three factors favor enrichment of the PMMA NPs at the free surface, which could help explain the higher experimental  $Z^*$  value compared to the theoretical values. Previously, theory and modeling studies corrected for chain-end effects in polymer melts (e.g., stars, branched, etc.) and described surface and substrate enrichment in athermal PNCs. <sup>7,10,14,42</sup> Nevertheless, a single, unified PNC

model that incorporates the contributions discussed herein remains elusive. One goal of this experimental study is to provide data that allow theorists to develop and test models that appropriately capture the surface and bulk thermodynamic contributions needed to accurately predict polymer-grafted NP surface segregation in PNCs.

# CONCLUSIONS

In this work, we show that polymer-grafted NPs initially welldispersed in a polymer matrix segregate on the free surface of a film upon thermal annealing within the one-phase region (i.e.,  $T < T_{LCST}$ ) of the phase diagram when the grafted polymer has a lower surface energy than that of the matrix polymer. Using AFM, we demonstrate that the grafted NP number density approaches  $517 \pm 36 \text{ NP}/\mu\text{m}^2$ , which is  $1.7 \times$  greater than the value of the as-cast 25/75 wt % PMMA-NP/SAN film (302  $\pm$ 24 NP/ $\mu$ m<sup>2</sup>) at the longest annealing time. In comparison, the number density of PNCs annealed in the two-phase region approaches plateau values of 593  $\pm$  26 and 620  $\pm$  25 NP/ $\mu$ m<sup>2</sup> at 170 and 190 °C, respectively. Here, the difference in the grafted-NP surface coverage is attributed to  $\gamma$  and  $\Delta \gamma$ competing with one another for NP surface enrichment in the one-phase region. In contrast,  $\chi$  and  $\Delta \gamma$  mutually enhance surface wetting in the two-phase region. The enrichment of grafted NPs at the free surface of the PNC films is further corroborated through cross-sectional TEM micro-graphs as a function of annealing time. Using GI-RBS, the evolution of the grafted NP surface excess in 25/75 wt % PMMA-NP/SAN films is observed as a function of annealing time. The temporal growth of the surface excess in the one-phase region is interpreted as a competition between entropic constraints, surface-energy differences of the constituents, and the Flory-Huggins interaction parameter,  $\chi$ . For the first time in a miscible binary PNC mixture, quantitative comparisons of this behavior are made with the predictions of prevailing theories derived for analogous polymer blends. Using two PMMA molecular weights corresponding to the brush and the effective radius of gyration of PMMA NPs (19 nm), the surface excess values for a PMMA/SAN blend are calculated to be 0.70 and 0.79 nm, respectively. These predictions are ca. 5× lower than the experimentally obtained Z\* value for PMMA NP/SAN, motivating the need for sophisticated models that capture the phase behavior and surface properties of more complicated PNC systems.

Additionally, the insights provided herein could be leveraged to design advanced materials where surface functionality needs to be decoupled from that of the bulk. Since the grafting densities of the NPs are high, the PMMA chains shield the silica NP core such that core-core interactions are effectively screened. The presented PNC morphologies are therefore dictated by the thermodynamic interactions of PMMA and SAN rather than core-core interactions between NPs. This has been previously discussed in detail by Maguire et al.<sup>26</sup> As such, changing the NP core should have no effect on the resulting phase behavior with everything else held constant. In addition to changing the NP core, manipulating the relative molecular weights of the matrix (P) and graft (N) molecular weights should result in various degrees of NP surface enrichment. For instance, the degree of surface enrichment is dependent on two main variables,  $\chi$  and  $\Delta \gamma$ , both of which are dependent on the molecular weights of the constituents. This has been demonstrated in an athermal system by Maillard et al., where the extent of surface segregation of hairy NPs and

their self-assembly into a variety of structures can be tuned by varying the number and the length of the grafted chains and the matrix chain length. 43 Furthermore, all experiments presented herein were performed at a fixed PNC concentration of 25/75 wt % PMMA NP/SAN. As such, we hypothesize that the presented  $Z^*$  values will change with NP loading based on previous work performed by Kramer et al. 15 Here, they demonstrated that the surface excess of the lower-surfaceenergy homopolymer in an isotopic polymer blend is highly dependent on the loading of that constituent. Therefore, aside from manipulating the dispersion state of the grafted NPs through thermal annealing, it is not unreasonable to think that the surface properties of the PNC film could be further manipulated through other means such as substitution of the NP core, varying the P/N ratio, or changing the composition of the PNC. The phenomenon presented in this study lends itself to the design of highly controlled spatial organization of NPs, particularly at interfaces, with broadly tunable property enhancements through intentional engineering and the polymer physics concepts presented herein.

#### ASSOCIATED CONTENT

# Supporting Information

The Supporting Information is available free of charge at https://pubs.acs.org/doi/10.1021/acs.macromol.2c00839.

Sample preparation, experimental methods, and additional figures as described in the text (PDF)

# AUTHOR INFORMATION

# **Corresponding Author**

Russell J. Composto – Department of Materials Science and Engineering, University of Pennsylvania, Philadelphia, Pennsylvania 19104, United States; oorcid.org/0000-0002-5906-2594; Email: composto@seas.upenn.edu

### **Authors**

Shawn M. Maguire — Department of Materials Science and Engineering, University of Pennsylvania, Philadelphia, Pennsylvania 19104, United States; Present Address: Department of Chemical and Biological Engineering, Princeton University, Princeton, New Jersey 08544, United States; orcid.org/0000-0002-5317-4990

John Derek Demaree – US Army Research Laboratory, Aberdeen Proving Ground, Maryland 21005, United States Michael J. Boyle – Department of Materials Science and Engineering, University of Pennsylvania, Philadelphia, Pennsylvania 19104, United States

Austin W. Keller – Department of Materials Science and Engineering, University of Pennsylvania, Philadelphia, Pennsylvania 19104, United States

Connor R. Bilchak — Department of Materials Science and Engineering, University of Pennsylvania, Philadelphia, Pennsylvania 19104, United States; Present Address: Department of Chemical Engineering, Manhattan College, Bronx, New York 10471, United States; Orcid.org/0000-0001-8815-1601

Cherie R. Kagan – Department of Materials Science and Engineering, University of Pennsylvania, Philadelphia, Pennsylvania 19104, United States; Department of Chemistry and Department of Electrical and Systems Engineering, University of Pennsylvania, Philadelphia,

Pennsylvania 19104, United States; oorcid.org/0000-0001-6540-2009

Christopher B. Murray — Department of Materials Science and Engineering, University of Pennsylvania, Philadelphia, Pennsylvania 19104, United States; Department of Chemistry, University of Pennsylvania, Philadelphia, Pennsylvania 19104, United States

Kohji Ohno — Department of Materials Science, Graduate School of Engineering, Osaka Metropolitan University, Sakai, Osaka 599-8531, Japan; orcid.org/0000-0002-1812-3354

Complete contact information is available at: https://pubs.acs.org/10.1021/acs.macromol.2c00839

#### **Author Contributions**

R.J.C. designed and supervised this work. S.M.M., J.D.D., M.J.B., C.R.B., and A.W.K., carried out experiments. S.M.M., J.D.D., and M.J.B. analyzed experimental results. S.M.M. prepared schematics. The manuscript was written and edited through contributions of all authors. All authors have given approval to the final version of the manuscript.

#### Notes

The authors declare no competing financial interest.

# ACKNOWLEDGMENTS

S.M.M., C.R.B., and R.J.C. were supported by the National Science Foundation Partnerships for International Research and Education Program (NSF-PIRE), grant #1545884. This work was also supported by the POLYMERS-DMR-1905912 (S.M.M., C.R.B., and R.J.C.) and MRSEC-DMR-1720530 (S.M.M., C.R.B., and R.J.C.) programs. M.J.B. acknowledges funding from the NSF Graduate Fellowship and NSF-CBET-1706014 (R.J.C. and M.J.B.). A.W.K., C.R.K., and C.B.M. acknowledge funding from the Semiconductor Research Corporation (SRC), Task 2797.001. The authors gratefully acknowledge the use of facilities and instrumentation (TGA, DSC, and DLS) supported by the Materials Science and Engineering Departmental Laboratory at the University of Pennsylvania. The authors thank Dr. Karen I. Winey and Dr. Zahra Fakhraai for use of their laboratory's ultramicrotome and atomic force microscope, respectively. The authors also acknowledge Dr. Robert A. Riggleman, Dr. Daeyeon Lee, and Dr. James F. Pressly for helpful discussions.

#### REFERENCES

- (1) Kumar, S. K.; Jouault, N.; Benicewicz, B.; Neely, T. Nanocomposites with Polymer Grafted Nanoparticles. *Macromolecules* **2013**, *46*, 3199–3214.
- (2) Bandyopadhyay, D.; Douglas, J. F.; Karim, A. Influence of C60 Nanoparticles on the Stability and Morphology of Miscible Polymer Blend Films. *Macromolecules* **2011**, *44*, 8136–8142.
- (3) Gupta, S.; Zhang, Q.; Emrick, T.; Balazs, A. C.; Russell, T. P. Entropy-Driven Segregation of Nanoparticles to Cracks in Multilayered Composite Polymer Structures. *Nat. Mater.* **2006**, *5*, 229–233.
- (4) Huang, J.; Xiao, Y.; Xu, T. Achieving 3-D Nanoparticle Assembly in Nanocomposite Thin Films via Kinetic Control. *Macromolecules* **2017**, *50*, 2183–2188.
- (5) Guillaume, O.; Geven, M. A.; Sprecher, C. M.; Stadelmann, V. A.; Grijpma, D. W.; Tang, T. T.; Qin, L.; Lai, Y.; Alini, M.; de Bruijn, J. D.; Yuan, H.; Richards, R. G.; Eglin, D. Surface-Enrichment with Hydroxyapatite Nanoparticles in Stereolithography-Fabricated Composite Polymer Scaffolds Promotes Bone Repair. *Acta Biomater.* **2017**, *54*, 386–398.

- (6) Mah, A. H.; Laws, T.; Li, W.; Mei, H.; Brown, C. C.; Ievlev, A.; Kumar, R.; Verduzco, R.; Stein, G. E. Entropic and Enthalpic Effects in Thin Film Blends of Homopolymers and Bottlebrush Polymers. *Macromolecules* **2019**, *52*, 1526–1535.
- (7) McGarrity, E. S.; Frischknecht, A. L.; Frink, L. J. D.; Mackay, M. E. Surface-Induced First-Order Transition in Athermal Polymer-Nanoparticle Blends. *Phys. Rev. Lett.* **2007**, *99*, 238302.
- (8) Mackay, M. E.; Tuteja, A.; Duxbury, P. M.; Hawker, C. J.; Van Horn, B.; Guan, Z.; Chen, G.; Krishnan, R. S. General Strategies for Nanoparticle Dispersion. *Science* **2006**, *311*, 1740–1743.
- (9) Krishnan, R. S.; Mackay, M. E.; Hawker, C. J.; Van Horn, B. Influence of Molecular Architecture on the Dewetting of Thin Polystyrene Films. *Langmuir* **2005**, *21*, 5770–5776.
- (10) Frischknecht, A. L.; Padmanabhan, V.; Mackay, M. E. Surface-Induced Phase Behavior of Polymer/Nanoparticle Blends with Attractions. *J. Chem. Phys.* **2012**, *136*, 164904.
- (11) Mitra, I.; Li, X.; Pesek, S. L.; Makarenko, B.; Lokitz, B. S.; Uhrig, D.; Ankner, J. F.; Verduzco, R.; Stein, G. E. Thin Film Phase Behavior of Bottlebrush/Linear Polymer Blends. *Macromolecules* **2014**, *47*, 5269–5276.
- (12) Lee, J. S.; Lee, N. H.; Peri, S.; Foster, M. D.; Majkrzak, C. F.; Hu, R.; Wu, D. T. Surface Segregation Driven by Molecular Architecture Asymmetry in Polymer Blends. *Phys. Rev. Lett.* **2014**, *113*, 225702.
- (13) Genzer, J.; Composto, R. J. Surface Segregation Amplification in Miscible Polymer Blends near Criticality. *Europhys. Lett.* **1997**, *38*, 171–176.
- (14) Wu, D. T.; Fredrickson, G. H. Effect of Architecture in the Surface Segregation of Polymer Blends. *Macromolecules* **1996**, 29, 7919–7930.
- (15) Jones, R. A. L.; Kramer, E. J.; Rafailovich, M. H.; Sokolov, J.; Schwarz, S. A. Surface Enrichment in an Isotopic Polymer Blend. *Phys. Rev. Lett.* **1989**, *62*, 280–283.
- (16) Genzer, J.; Faldi, A.; Oslanec, R.; Composto, R. J. Surface Enrichment in a Miscible Polymer Blend: An Experimental Test of Self-Consistent Field and Long-Wavelength Approximation Models. *Macromolecules* 1996, 29, 5438–5445.
- (17) Oslanec, R.; Genzer, J.; Faldi, A.; Composto, R. J.; Garrett, P. D. Surface Enrichment in a Miscible Random Copolymer Blend: Influence of Polydispersity and Architecture. *Macromolecules* **1999**, 32, 4098–4105.
- (18) Zhao, X.; Zhao, W.; Sokolov, J.; Rafailovich, M. H.; Schwarz, S. A.; Wilkens, B. J.; Jones, R. A. L.; Kramer, E. J. Determination of the concentration profile at the surface of deuterated polystyrene/hydrogenated polystyrene blends using high-resolution ion scattering techniques. *Macromolecules* **1991**, *24*, 5991–5996.
- (19) Jones, R. A. L.; Kramer, E. J. The Surface Composition of Miscible Polymer Blends. *Polymer* **1993**, *34*, 115–118.
- (20) Pan, D. H. K.; Prest, W. M. Surfaces of polymer blends: X-ray photoelectron spectroscopy studies of polystyrene/poly(vinyl methyl ether) blends. *J. Appl. Phys.* **1985**, *58*, 2861–2870.
- (21) Norton, L. J.; Kramer, E. J.; Bates, F. S.; Gehlsen, M. D.; Jones, R. A. L.; Karim, A.; Felcher, G. P.; Kleb, R. Neutron Reflectometry Study of Surface Segregation in an Isotopic Poly(Ethylenepropylene) Blend: Deviation from Mean-Field Theory. *Macromolecules* **1995**, 28, 8621–8628.
- (22) Composto, R. J.; Stein, R. S.; Kramer, E. J.; Jones, R. A. L.; Mansour, A.; Karim, A.; Felcher, G. P. Surface Enrichment In Polymer Blends A Neutron Reflection Test. *Phys. B* **1989**, *156–157*, 434–436.
- (23) Forrey, C.; Koberstein, J. T.; Pan, D. H. Surface Segregation in Miscible Blends of Polystyrene and Poly(Vinylmethyl Ether): Comparison of Theory and Experiment. *Interface Sci.* **2003**, *11*, 211–223.
- (24) Cowie, J. M. G.; Devlin, B. G.; McEwen, I. J. Surface Enrichment in PS/PVME Blends: 2. The Effect of Specific Interactions in the Bulk Mixture. *Polymer* **1993**, *34*, 4130–4134.
- (25) Maguire, S. M.; Boyle, M. J.; Bilchak, C. R.; Demaree, J. D.; Keller, A. W.; Krook, N. M.; Ohno, K.; Kagan, C. R.; Murray, C. B.;

- Rannou, P.; Composto, R. J. Grafted Nanoparticle Surface Wetting during Phase Separation in Polymer Nanocomposite Films. *ACS Appl. Mater. Interfaces* **2021**, *13*, 37628–37637.
- (26) Maguire, S. M.; Krook, N. M.; Kulshreshtha, A.; Bilchak, C. R.; Brosnan, R.; Pana, A. M.; Rannou, P.; Maréchal, M.; Ohno, K.; Jayaraman, A.; Composto, R. J. Interfacial Compatibilization in Ternary Polymer Nanocomposites: Comparing Theory and Experiments. *Macromolecules* **2021**, *54*, 797–811.
- (27) Ohno, K.; Morinaga, T.; Koh, K.; Tsujii, Y.; Fukuda, T. Synthesis of Monodisperse Silica Particles Coated with Well-Defined, High-Density Polymer Brushes by Surface-Initiated Atom Transfer Radical Polymerization. *Macromolecules* **2005**, *38*, 2137–2142.
- (28) Zhou, J.; Jiang, Y.; Doi, M. Cross Interaction Drives Stratification in Drying Film of Binary Colloidal Mixtures. *Phys. Rev. Lett.* **2017**, *118*, 108002.
- (29) Howard, M. P.; Nikoubashman, A.; Panagiotopoulos, A. Z. Stratification in Drying Polymer-Polymer and Colloid-Polymer Mixtures. *Langmuir* **2017**, 33, 11390–11398.
- (30) Miyagi, K.; Mei, H.; Terlier, T.; Stein, G. E.; Verduzco, R. Analysis of Surface Segregation of Bottlebrush Polymer Additives in Thin Film Blends with Attractive Intermolecular Interactions. *Macromolecules* **2020**, *53*, 6720–6730.
- (31) Cheng, S.; Grest, G. S. Dispersing Nanoparticles in a Polymer Film via Solvent Evaporation. ACS Macro Lett. **2016**, *5*, 694–698.
- (32) Carroll, B.; Bocharova, V.; Carrillo, J. M. Y.; Kisliuk, A.; Cheng, S.; Yamamoto, U.; Schweizer, K. S.; Sumpter, B. G.; Sokolov, A. P. Diffusion of Sticky Nanoparticles in a Polymer Melt: Crossover from Suppressed to Enhanced Transport. *Macromolecules* **2018**, *51*, 2268–2275.
- (33) Lin, C. C.; Griffin, P. J.; Chao, H.; Hore, M. J. A.; Ohno, K.; Clarke, N.; Riggleman, R. A.; Winey, K. I.; Composto, R. J. Grafted Polymer Chains Suppress Nanoparticle Diffusion in Athermal Polymer Melts. J. Chem. Phys. 2017, 146, 203332.
- (34) Griffin, P. J.; Bocharova, V.; Middleton, L. R.; Composto, R. J.; Clarke, N.; Schweizer, K. S.; Winey, K. I. Influence of the Bound Polymer Layer on Nanoparticle Diffusion in Polymer Melts. *ACS Macro Lett.* **2016**, *5*, 1141–1145.
- (35) Bailey, E. J.; Winey, K. I. Dynamics of Polymer Segments, Polymer Chains, and Nanoparticles in Polymer Nanocomposite Melts: A Review. *Prog. Polym. Sci.* **2020**, *105*, 101242.
- (36) Boyle, M. J.; Maguire, S. M.; Rose, K. A.; Lee, D.; Composto, R. J. Nanoparticle Transport Through Polymers and Along Interfaces. In *Macromolecular Engineering*; Hadjichristidis, N., Gnanou, Y., Matyjaszewski, K., Muthukumar, M., Eds.; Wiley, 2022; pp 1–71.
- (37) Schmidt, I.; Binder, K. Model Calculations for Wetting Transitions in Polymer Mixtures. *J. Phys.* **1985**, *46*, 1631–1644.
- (38) Higashida, N.; Kressler, J.; Inoue, T. Lower Critical Solution Temperature and Upper Critical Solution Temperature Phase Behavior in Random Copolymer Blends: Poly(Styrene-Co-Acrylonitrile)/Poly(Methyl Methacrylate) and Poly(Styrene-Co-Acrylonitrile)/Poly(e-Caprolactone). *Polymer* 1995, 36, 2761–2764.
- (39) Chung, H.; Kim, J.; Ohno, K.; Composto, R. J. Controlling the Location of Nanoparticles in Polymer Blends by Tuning the Length and End Group of Polymer Brushes. *ACS Macro Lett.* **2012**, *1*, 252–256.
- (40) Koski, J. P.; Krook, N. M.; Ford, J.; Yahata, Y.; Ohno, K.; Murray, C. B.; Frischknecht, A. L.; Composto, R. J.; Riggleman, R. A. Phase Behavior of Grafted Polymer Nanocomposites from Field-Based Simulations. *Macromolecules* **2019**, *52*, 5110–5121.
- (41) Bhatia, Q. S.; Pan, D. H.; Koberstein, J. T. Preferential Surface Adsorption in Miscible Blends of Polystyrene and Poly(Vinyl Methyl Ether). *Macromolecules* 1988, 21, 2166–2175.
- (42) Wu, D. T.; Fredrickson, G. H.; Carton, J.-P.; Ajdari, A.; Leibler, L. Distribution of Chain Ends at the Surface of a Polymer Melt: Compensation Effects and Surface Tension. *J. Polym. Sci., Part B: Polym. Phys.* **1995**, 33, 2373–2389.
- (43) Maillard, D.; Kumar, S. K.; Fragneaud, B.; Kysar, J. W.; Rungta, A.; Benicewicz, B. C.; Deng, H.; Brinson, L. C.; Douglas, J. F. Mechanical Properties of Thin Glassy Polymer Films Filled with

Spherical Polymer-Grafted Nanoparticles. Nano Lett. 2012, 12, 3909–3914.